

# Geometrically Taming Dynamical Entanglement Growth in Purified Quantum States

Tim Pokart,<sup>1,\*</sup> Carl Lehmann,<sup>1,2</sup> and Jan Carl Budich<sup>1,2,†</sup>

<sup>1</sup>*Institute of Theoretical Physics, Technische Universität Dresden*

<sup>2</sup>*Würzburg-Dresden Cluster of Excellence ct.qmat, 01062 Dresden, Germany*

(Dated: September 18, 2023)

Entanglement properties of purified quantum states are of key interest for two reasons. First, in quantum information theory minimally entangled purified states define the Entanglement of Purification as a fundamental measure for the complexity of the corresponding physical mixed state. Second, dynamical entanglement growth in purified states represents the main bottleneck for calculating dynamical physical properties on classical computers in the framework of tensor network states. Here, we demonstrate how geometric methods including parallel transport may be harnessed to drastically reduce such dynamical entanglement growth, and to obtain a general prescription for maintaining (locally) optimal entanglement entropy when time-evolving a purified state. Adapting and extending by higher order skew corrections the notion of Uhlmann geometric phases, we thus reveal the relation between dynamical entanglement growth and the geometry of the Hilbert-Schmidt bundle as the mathematical foundation of purified states. With benchmarks on a non-integrable spin chain model, we compare the computational performance of matrix product state algorithms based on our present geometric disentangling method to previous approaches for taming entanglement growth in purified states. Our findings provide numerical evidence that geometric disentanglers are at least competitive and even outperform existing techniques in an extended parameter regime relevant to the practical calculation of dynamical response functions. To exclude the effect of avoidable algorithmic imperfections, we provide a numerically exact analysis for systems of moderate size.

## I. INTRODUCTION

Disentangling different forms of correlation and complexity in mixed quantum states [1–3] represents a salient challenge [4–7] in quantum science, both at a fundamental quantum information level and at a practical computational one. In the context of many-body physics, thermal equilibrium states exhibiting a subtle interplay of both classical and genuine quantum correlations are ubiquitous examples of mixed states [8, 9]. A versatile platform for unraveling mixed states is provided by the notion of purification [10, 11], i.e. their representation as pure states  $|\psi\rangle$  in a total Hilbert space  $\mathcal{H} = \mathcal{H}_S \otimes \mathcal{H}_A$ , consisting of the (physical) system state space  $\mathcal{H}_S$  extended by an auxiliary space  $\mathcal{H}_A$ . Besides their conceptual importance for entanglement measures such as entanglement of purification (EOP) [12], purified states are also an integral part of the computational toolbox for simulating quantum dynamics on a classical computer using tensor network states [13].

Specifically, given a purification  $|\psi\rangle \in \mathcal{H}$ , the corresponding physical mixed state  $\rho$  is obtained by tracing out the auxiliary degrees of freedom, i.e.  $\rho = \text{tr}_A |\psi\rangle\langle\psi|$ . This naturally introduces a giant gauge degree of freedom [14], since any unitary transformation  $U_A$  within the auxiliary space  $\mathcal{H}_A$  will leave  $\rho$  as the result of the partial trace unaffected. However, for a different partition  $\mathcal{H} = \mathcal{H}_L \otimes \mathcal{H}_R$  involving the division of the physical system into left and right spatial regions (see Fig. 1a), the choice of  $U_A$  may have a drastic effect on the entan-

glement properties of  $|\psi\rangle$ . Yet, the minimal entropy of say  $\rho_L = \text{tr}_R |\psi\rangle\langle\psi|$  obtained by an optimal choice of  $U_A$  defines the EOP [15], a physical property of  $\rho$  encoding its gauge-independent correlations. Below, we explore the potential of concepts from differential geometry such as geometric phases for solving the outstanding problem of finding an optimal gauge  $U_A$  to mitigate entanglement growth in quantum dynamics [16].

Our main focus is on investigating dynamical correlation functions of the form

$$C(t) = \langle X(t)Y \rangle_\beta = \text{tr}[X(t)Y\rho_\beta], \quad (1)$$

where a mixed quantum state naturally occurs in the form of a thermal state operator  $\rho_\beta = Z^{-1} \exp(-\beta H)$  of a system governed by the Hamiltonian  $H$  and with the partition function  $Z = \text{tr} \exp(-\beta H)$  at inverse temperature  $\beta = 1/T$ . In Eq. (1),  $t$  denotes time such that  $X(t) = U^\dagger(t)XU(t)$ ,  $Y = Y(0)$  are operators acting on  $\mathcal{H}_S$  in the Heisenberg picture. When purifying Eq. (1), a typical choice is to model the auxiliary system as a duplicate of the physical system, i.e.  $\mathcal{H}_S \cong \mathcal{H}_A$  (see Fig. 1a).

Impressive computational progress on evaluating dynamical correlation functions has been made with the advent of tensor network (TN) methods such as MPS approaches [10, 17–20]. There, the entanglement of the purified state  $|\psi\rangle$  represents the main bottleneck [21, 22] to the quality of numerical data on physical observables. This is because the computational effort of MPS simulations, as measured by the required size  $\chi$  of the tensors (bond dimension), grows exponentially with the entanglement entropy  $S_L(t) = -\text{tr}[\rho_L(t) \log \rho_L(t)]$  (see Fig. 1a), i.e.  $\chi(t) \geq \exp(S_L(t))$  [23]. While  $S_L$  is bounded from below by the EOP relating to the inherent complexity

\* tim.pokart@tu-dresden.de

† jan.budich@tu-dresden.de

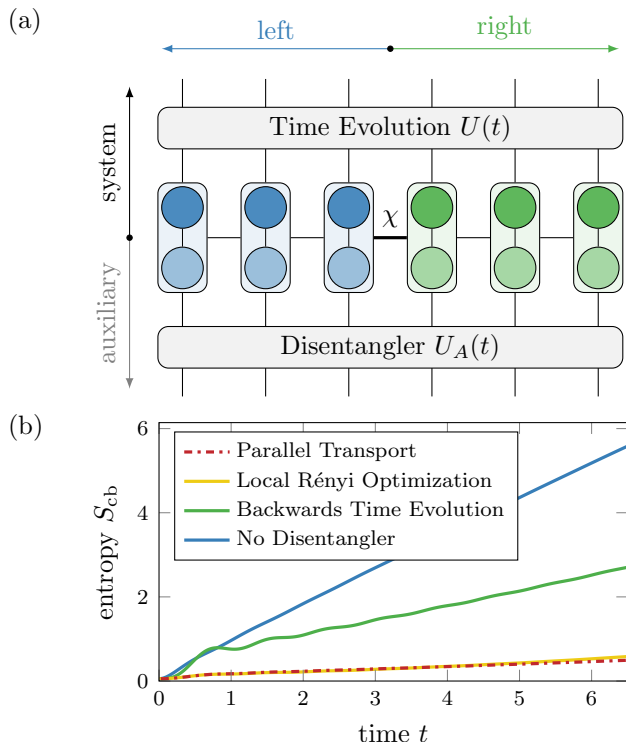


FIG. 1. (a) Illustration of an MPS purifying a mixed state defined on a lattice of six physical sites (darker) by coupling them to a duplicate of auxiliary sites (lighter). The central bond dimension  $\chi$  directly relates to the entanglement entropy  $S_{cb}$  of a spatial bipartition into the left (blue) and right (green) half of the total system. On the system (auxiliary) degrees of freedom a time-evolution (disentangling) operator  $U(t)$  ( $U_A(t)$ ) is applied, with drastic effects on entanglement properties. (b)  $S_{cb}(t)$  of the TFI chain (see Eq. (20)) for different disentanglers  $U_A(t)$  applied after perturbing a thermal state at by applying a spin flip  $X_c$  at a central site. Specifically, the parallel-transport disentangler introduced here is compared to several established methods. Parameters are  $N = 200 = N_S + N_A$ ,  $\beta = 0.2$ ,  $J_x = -1.0$ ,  $J_z = -0.1$  and  $h = -1.0$ .

of the physical state, practically saturating this bound by a gauge choice  $U_A(t)$  is a hard optimization problem the exact solution to which remains elusive. However, significant progress for mitigating dynamical entanglement growth by means of gauge (or disentangler)  $U_A(t)$  has been reported based on heuristic arguments [21, 24] and numerical optimization of a variational  $U_A(t)$  consisting of local gates [25], respectively.

Here, we report on our results of using as a guiding principle for optimizing the disentangler  $U_A(t)$  geometric methods including Uhlmann parallel transport of purifications [26, 27] and higher order corrections derived below. As parallel transport amounts to applying the least change to  $|\psi(t)\rangle$  that is compatible with the correct physical trajectory  $\rho(t)$ , it is quite intuitive that this helps to avoid creating unnecessary correlations in  $|\psi(t)\rangle$  induced by a poor gauge. More quantitatively, we indeed find that parallel transport of the purified state substantially

reduces entanglement, and is at least competitive with numerically more costly brute force numerical optimization methods [25] (see Fig. 1b). Moreover, we find that parallel transport can be extended by skew-corrections accounting for differential deviations from a locally optimal entropy  $S_L(t)$  to achieve even better results (see Fig. 4), which highlights the far reaching potential of geometric optimization. Practically, parallel transport amounts to computing an effective Hamiltonian  $G$  that generates the auxiliary time evolution  $U_A(t)$ . Interestingly, we find that approximations to  $G$  such as its value at infinite temperature can lead to very promising computational results that outperform existing methods for paradigmatic non-integrable models (see Fig. 7). Our general findings are corroborated by numerical benchmark simulations using both exact diagonalization (ED) and MPS methods.

*Outline.* This article is structured as follows: In Section II the purification approach to represent mixed states by introducing an auxiliary Hilbert space is briefly reviewed in the differential geometric framework of the Hilbert-Schmidt bundle. In this context, a parallel transport condition is derived and adapted to the computation of dynamical correlation functions (see Section II A). In Section II B these concepts are linked to the dynamical growth of entanglement under time evolution, and higher order corrections to plain parallel transport are derived that allow for maintaining (locally) optimal entanglement. Thereafter, in Section III, based on a paradigmatic model Hamiltonian of a non-integrable spin chain, numerical results in the framework of ED (see Section III A) as well as MPS (see Section III B) are provided. Finally, a concluding discussion is presented in Section IV.

## II. GEOMETRIC PERSPECTIVE ON ENTANGLEMENT OF PURIFICATIONS

To purify a (mixed) quantum state described by the density matrix  $\rho$  in the *physical* Hilbert space  $\mathcal{H}_S$ , an *auxiliary* Hilbert space  $\mathcal{H}_A$  is introduced such that a pure state  $|\psi\rangle \in \mathcal{H}$  in the *total* Hilbert space  $\mathcal{H} = \mathcal{H}_S \otimes \mathcal{H}_A$  fulfills

$$\rho = \text{tr}_A |\psi\rangle\langle\psi| \quad (2)$$

with  $\text{tr}_A$  denoting the partial trace of the auxiliary Hilbert space. This construction admits to an interesting gauge degree of freedom: given a unitary  $U_A$  acting on  $\mathcal{H}_A$ , the transformed purification  $\mathbb{I} \otimes U_A |\psi\rangle$  yields the same state  $\rho$  as is clear from Eq. (2). In Section II A, a brief synopsis of how this gauge freedom is used to derive a parallel transport condition [26] is presented, singling out the shortest path a purification can traverse in  $\mathcal{H}$  during a time evolution constrained by the time-dependent physical state  $t \mapsto \rho(t)$  in  $\mathcal{H}_S$ . Then, in Section II B, we relate this parallel transport prescription and higher order corrections to entanglement growth in quantum dynamics.

For our geometric analysis, we find it helpful to define the auxiliary space as the dual of the physical space, i.e.

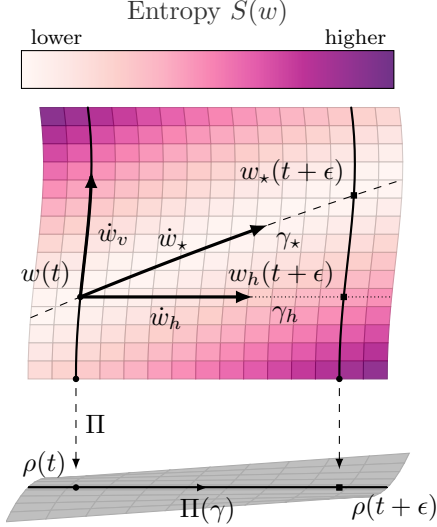


FIG. 2. Visualization of the relation between geometry and entanglement landscape in the Hilbert-Schmidt bundle of purifications  $w$ . In a slice of the bundle that projects to a path  $t \mapsto \rho(t)$  of physical mixed states, the tangent vectors  $\dot{w}$  of several distinguished paths  $\gamma$  are shown, while the entropy  $S(w)$  is quantified by the color code. Specifically, the vertical component  $\dot{w}_v$  originating from transport within a given fiber  $\Pi^{-}(\rho(t))$ , the horizontal direction  $\dot{w}_h$  corresponding to Uhlmann parallel transport, and the entanglement optimal direction  $\dot{w}_*$  following the valley of the entropy are depicted. Importantly, for an initial state that is minimally entangled within its fiber  $\Pi^{-}(\rho(t))$ , the optimal route (denoted by  $\gamma_*$ ) is not purely horizontal (cf.  $\gamma_h$ ), since the entanglement landscape is skewed. Locally however, without further knowledge of the curvature, the horizontal path along  $\gamma_h$  (dotted) is the best guess for the direction to move in to leading order.

$\mathcal{H}_A = \mathcal{H}_S^*$  [28]. Under this definition, the purification is conveniently represented as a matrix  $w \in \mathcal{H}_S \otimes \mathcal{H}_S^*$  known as a Hilbert-Schmidt operator. The Hilbert-Schmidt operator  $w$  is equivalent to the conventional purification  $|\psi\rangle \in \mathcal{H}_S \otimes \mathcal{H}_S$  in the sense of the following duality in Schmidt decomposition [29]:

$$|\psi\rangle = \sum_i \sqrt{\lambda_i} |\phi_i\rangle |\alpha_i\rangle \mapsto w = \sum_i \sqrt{\lambda_i} |\phi_i\rangle \langle \alpha_i|, \quad (3)$$

defines a natural isomorphism between the two approaches to purification through flipping the auxiliary basis states from ket to bra type. Tracing out the auxiliary degrees of freedom to compute the physical density matrix then simply amounts to a matrix multiplication such that Eq. (2) becomes  $\rho = ww^\dagger$ . Note that a unitary  $U_A$  acting on  $\mathcal{H}_S^*$  still represents a gauge degree of freedom, since  $\tilde{w} = wU_A$  corresponds to the same state  $\rho = ww^\dagger = \tilde{w}\tilde{w}^\dagger$ .

### A. Parallel Transport for Correlation Functions

Turning to differential geometry, the purification may be formalized [30, 31] as a principal fiber bundle called

the Hilbert-Schmidt bundle (see Fig. 2) via the projection

$$\Pi : w \mapsto \rho = ww^\dagger \quad (4)$$

mapping elements  $w$  of the total space of (invertible) Hilbert-Schmidt operators to density matrices  $\rho$  of full rank (e.g. thermal states) as elements of the physical base space (see e.g. [31] for a more detailed discussion). The typical fiber (gauge group) consists of the unitary transformations  $U_A$  on the auxiliary (dual) space  $\mathcal{H}_A = \mathcal{H}_S^*$ . In addition, the Hilbert-Schmidt bundle has a metric structure as induced by the Hilbert-Schmidt inner product

$$(w, v) = \text{tr } w^\dagger v \quad (5)$$

of two matrices  $w$  and  $v$ . Finally, the mapping  $\rho \rightarrow \sqrt{\rho}$  uniquely defines a global section on the Hilbert-Schmidt bundle as a consequence of the polar decomposition of  $w$ , thus implying a topologically trivial global product structure.

Parallel transport and geometric phases in quantum mechanics are best known for pure states resulting in the accumulation of a Berry phase [32] when the Hamiltonians parameters are varied adiabatically along a path. Uhlmann [26, 27] derived a way to extend the Berry phase formalism to generic density matrices. Given a path of purifications  $\gamma : t \mapsto w(t)$  in the Hilbert-Schmidt bundle, an arbitrary element  $\dot{w} \equiv \frac{d}{dt}w$  of the tangent space at  $w$  can be decomposed into a vertical part  $\dot{w}_v$  and a horizontal part  $\dot{w}_h$  with respect to the path  $\gamma$ . To construct the vertical vector  $\dot{w}_v$  [31, 33], we consider at first a path  $\gamma' : t \mapsto w(t) = w_0 U_A(t)$ , which stays within a single fiber of the bundle. The unitary operation  $U_A(t)$  describing the path, is at  $t = 0$  generated by a Hermitian matrix  $g$  such that  $U_A(t) = \exp(-itg)$ . Then, the vertical vectors at  $t = 0$  are given by

$$\dot{w}_v = \frac{d}{dt} w_0 e^{-itg} \big|_{t=0} = -i w_0 g. \quad (6)$$

The respective horizontal vectors  $\dot{w}_h$  along the unrestricted path  $\gamma$  can then be defined via the scalar product Eq. (5) requiring orthogonality with respect to the vertical components such that

$$0 = (\dot{w}_v, \dot{w}_h) + (\dot{w}_h, \dot{w}_v) = -i \text{tr}(g(\dot{w}_h^\dagger w - w^\dagger \dot{w}_h)), \quad (7)$$

irrespective of the hermitian matrix  $g$ . Hence, a tangent vector  $\dot{w}$  of an arbitrary path is horizontal with respect to a purification  $w$  if and only if [26]

$$\dot{w}^\dagger w - w^\dagger \dot{w} = 0. \quad (8)$$

This condition can be formally solved for a general time dependent invertible density matrix  $\rho(t) = w(t)w^\dagger(t)$ . The resulting unitary part  $\mathcal{U}(t)$  of the amplitude  $t \mapsto w(t) = \sqrt{\rho(t)}\mathcal{U}(t)$  along a parallel transported path is given by [31, 34]

$$\mathcal{U}(t) = \mathcal{T} e^{-\int_0^t \mathcal{A}} U_A(0), \quad (9)$$

where  $\mathcal{T}$  denotes time-ordering and the Uhlmann connection  $\mathcal{A} = \mathcal{U}(d\mathcal{U})^\dagger$  may be obtained as the solution to a Lyapunov equation yielding [26]

$$\mathcal{A} = \int_0^\infty d\tau e^{-\tau\rho(t)} [\sqrt{\rho(t)}, d\sqrt{\rho(t)}] e^{-\tau\rho(t)}. \quad (10)$$

The total phase change  $H_\gamma = \mathcal{U}(t)\mathcal{U}^\dagger(0)$  is known as the Uhlmann geometric phase (holonomy).

For our purposes, an important special case is to assume a time-evolution  $t \mapsto \rho(t) = e^{-iHt}\rho(0)e^{iHt}$  generated by a time-independent physical Hamiltonian  $H$ . The time evolution on the auxiliary space then simplifies to  $\mathcal{U}(t) = e^{-iHt}e^{-iGt}\mathcal{U}(0)$  with the time-independent auxiliary Hamiltonian  $G$  that is of the explicit form

$$G = -2 \int_0^\infty d\tau e^{-\rho(0)\tau} \sqrt{\rho(0)} H \sqrt{\rho(0)} e^{-\rho(0)\tau}. \quad (11)$$

The equivalent Lyapunov equation in this case reads as

$$AG + GA + Q = 0 \quad (12)$$

with  $A = -\rho(0)$  and  $Q = -2\sqrt{\rho(0)}H\sqrt{\rho(0)}$ .

To harness parallel transport for the calculation of correlation functions, building on [25] we approach Eq. (1) with the help of two new correlation functions

$$C_\pm(\epsilon, t) \equiv \text{tr}[X(t)\rho_\pm] \quad (13)$$

with  $\rho_- = e^{-i\epsilon Y}\rho e^{i\epsilon Y^\dagger}$  and  $\rho_+ = e^{\epsilon Y}\rho e^{\epsilon Y^\dagger}$  such that the initial correlation function Eq. (1) is obtained from

$$C(t) = \frac{1}{2} \partial_\epsilon (C_+(\epsilon, t) + iC_-(\epsilon, t))|_{\epsilon=0}. \quad (14)$$

Now, since  $\rho_\pm$  are still Hermitian matrices of full rank, their purification  $w_\pm$  is well defined up to the aforementioned gauge degree of freedom  $U_A$ , and

$$C_\pm(t) = \text{tr}[w_\pm^\dagger X(t)w_\pm] = \text{tr}[U_A^\dagger(t)w_\pm^\dagger X(t)w_\pm U_A(t)] \quad (15)$$

are gauge invariant functions due to the cyclic invariance of the trace. Hence, gauge-optimizing the time-dependent purifications  $\tilde{w}_\pm(t) = U(t)w_\pm U_A(t)$  represents a well defined problem that can be directly addressed using the geometric toolbox of parallel transport. This construction conveniently solves the phase matching problem discussed in Ref. [25], since the same  $U_A(t)$  enters  $C_\pm$  via both  $\tilde{w}_\pm$  and  $\tilde{w}_\pm^\dagger$ .

We now discuss several important limits of Eq. (11). First, both in the case of a static correlation function, i.e.  $Y = \mathbb{I}$  in Eq. (1), and in the zero temperature limit  $\beta = \infty$  ( $T = 0$ ), we find that  $G = -H$ , i.e. the program of parallel transport reduces to backward time evolution in the sense of Ref. [21]. This corroborates the theoretical foundation of the heuristically introduced backward time evolution approach. Second, the limit of infinite temperature  $\beta = 0$

( $T = \infty$ ) in Eq. (11) for which the auxiliary Hamiltonian assuming a unitary operator  $Y$  (cf. Eq. (1)) reads as

$$G = -Y^\dagger H Y. \quad (16)$$

This practically amounts to applying the (conjugate transposed) operator on the auxiliary space and time evolving the auxiliary degrees of freedom with the system Hamiltonian. Remarkably, as shown in Section III B, the infinite temperature limit in Eq. (16) yields a simple and widely applicable approximation even for physical states at finite temperature.

## B. Navigating the Entanglement Landscape Beyond Plain Parallel Transport

In the total space of purifications  $w$ , one may define an entanglement entropy function  $S(w)$  (see Fig. 2 for an illustration), e.g. representing the von Neumann entanglement entropy of the left-right decomposition illustrated in Fig. 1a. The subject of interest is then how  $S$  changes for small variations of  $w$  and in particular, how purifications of minimal entropy within their individual fiber  $\Pi^-(\rho)$  evolve along cross-sections (tantamount to gauge choices  $U_A(t)$ ).

Generally speaking, reaching the EOP  $E_p(\rho)$  as the principle lower bound on the entropy of interest  $S(w)$  for any purification  $w$  (with  $\rho = ww^\dagger$ ) represents the ultimate goal of any disentangler.  $E_p(\rho)$  is bounded by a Fannes-type inequality [35–37] that reads as [12]

$$|E_p(\rho) - E_p(\rho + d\rho)| \leq A \|d\rho\| - \|d\rho\| \log \|d\rho\|, \quad (17)$$

with a constant  $A$  depending on the specific Hilbert space under investigation and  $\|d\rho\|$  the length of the small deviation  $d\rho$  from  $\rho$  as measured by the Bures distance [38]. The Bures distance is defined on the Hilbert-Schmidt bundle as the minimal path length [39]

$$\|d\rho\| = \min_\gamma \int_\gamma \sqrt{(\dot{w}, \dot{w})} dt \quad (18)$$

for paths  $\gamma$  in the Hilbert-Schmidt bundle from purifications of  $\rho$  to  $\rho + d\rho$ . This length is precisely minimized by  $\gamma$  fulfilling the parallel transport condition Eq. (8) [30, 39]. Therefore, from Eq. (18) alone, it is clear that parallel transported changes in the purified state  $w$  translate to small changes in the entropy function as bounded by Eq. (17). In this sense, minimizing Eq. (18) along a physical path is intuitively favorable for mitigating dynamical entanglement growth. However, Eq. (17) does not provide a monotonous one-to-one relation between entanglement growth and change of the purification, and we indeed find that the plain parallel transport prescription Eq. (8) needs refinement to reveal a comprehensive geometric perspective on the entanglement entropy, as detailed in the following.

An optimal path  $\gamma_* : t \mapsto w_*(t)$  of purifications in the Hilbert-Schmidt bundle is distinguished by starting

from a purification  $w_*(0)$ , which is minimally entangled within the initial fiber  $\Pi^-(\rho(0))$  with  $\rho(0) = w_*(0)w_*^\dagger(0)$  (optimal initial gauge), and is then transported such that the entanglement remains in a minimum within the fibers  $\Pi^-(\rho(t))$  at any later point in time. To formalize this situation, we express the entropy  $S(t, \{\theta_i\})$  by parameterizing the purification  $w(t, \{\theta_i\})$  in terms of time  $t$ , and the parameters  $\theta_i$  of the linear combination of generators  $g_i$  describing the position along the fiber, such that  $w(t, \{\theta_i\}) = e^{-iHt}w(0)e^{-i\sum_i \theta_i g_i}$ . The initially minimal entanglement entropy then requires a vanishing gradient  $\partial_i S|_{w_*} = 0$  in the local parameters at the starting position. In order for the purification to continue to be locally optimal during the transport, this stationarity needs to persist, i.e. the path  $\gamma_*$  needs to evolve along the valley of minimal  $S$  in the total space, which is satisfied if

$$\frac{d}{dt}\partial_i S = \partial_i \partial_t S + (\partial_i \partial_j S)\dot{\theta}_j = 0. \quad (19)$$

Eq. (19) may be seen as the equation of motion governing entanglement-optimized transport of purifications. The solutions  $\gamma_*$  to Eq. (19) generically deviate slightly, for long times sometimes significantly, from the horizontally lifted purifications  $\gamma_h$ , i.e. the solutions to the plain parallel transport condition Eq. (8) (see Fig. 2 for an illustration). We refer to these deviations as *skew corrections* to parallel transport.

However, due to the rapid (exponential in system size) growth of the number of parameters  $\theta_i$ , a numerically exact solution to Eq. (19) is generically hard to obtain, except for small systems (see Section III A). Therefore, since an initially optimal purification implies that the Hessian  $\partial_i \partial_j S$  is positive definite such that generic movements along the vertical direction locally increase entanglement, the best direction to move in without further (higher order) information is the purely horizontal one of parallel transport, which can be efficiently determined as is discussed in Section II A and numerically exemplified in Section III.

In summary, the above analysis provides two key insights explaining with theory the success in mitigating dynamical entanglement growth (see Section III for numerical data) of our present geometric approach. First, plain parallel transport goes a long way to mitigate dynamical entanglement growth since its minimal changes to the purified state result in limited changes to the entanglement entropy. Second, maintaining a minimum of entanglement entropy along a physical path amounts to solving a conceptually simple but numerically challenging equation of motion (see Eq. (19)).

A remarkable simplification again occurs in the infinite temperature limit. There, the exact expression for the parallel transport generator  $G$  (see Eq. (16)) is found to also solve Eq. (19), i.e. no skew corrections to parallel transport occur. In addition, since the infinite temperature state does not contain any spatial entanglement, the dynamics is guaranteed to start at the global optimum of the entanglement entropy landscape. This favorable

stability of Eq. (16) provides theoretical intuition for our numerical finding (see Section III B) that using the infinite temperature value of  $G$  even at finite temperature provides a quite powerful and simple approximation.

### III. HARNESSING MIXED STATE GEOMETRY FOR COMPUTATIONAL METHODS

We now study the consequences of the above geometric analysis on the computation of correlation functions (see Eq. (1)) on a classical computer, both at a conceptual level of entanglement dynamics and regarding practical implications for TN method development, where entanglement growth represents the main limitation to simulating time-evolution of quantum many-body systems. In the following, we compare our geometric disentangling method to two major previous approaches: First, the heuristic idea of applying the physical time-evolution backwards on the auxiliary system as a disentangler [21, 24, 40], which is both popular and widely used due to its simplicity and effectiveness in significantly mitigating entanglement [22, 41–43]. Second, the variational approach of approximating the global (on the auxiliary system) gauge degree of freedom  $U_A(t)$  as a temporal series of local gates coupling two neighboring sites, and determining the parameters of those gates by solving an optimization problem for the (second) Rényi entropy at every time-step [25]. While computationally quite costly, this second approach in principle has the potential to further reduce the entanglement entropy beyond the backward time-evolution method for certain scenarios.

To obtain a quantitative comparison of our geometric construction to previous work in the context of a concrete microscopic model system, we focus on the non-integrable extension of the transverse field Ising model studied in Ref. [25] as a generic workhorse Hamiltonian. For  $N_S$  spin-1/2 sites arranged as a one-dimensional lattice (forming the system  $\mathcal{H}_S$ ), the physical system is governed by the Hamiltonian

$$H = \sum_{\langle i,j \rangle} (J_x X_i X_j + J_z Z_i Z_j) + h \sum_i Z_i, \quad (20)$$

subject to open boundary conditions. Here  $X_i, Y_i$  and  $Z_i$  represent the three components of the spin operator at site  $i$  with  $\langle i, j \rangle$  denoting nearest neighbors. Unless explicitly stated otherwise, we choose  $J_x = -1.0$ ,  $J_z = -0.1$  and  $h = -1.0$  for the coupling parameters, and consider for the average in Eq. (1) a thermal state at inverse temperature  $\beta = 0.2$ , which is created by purifying the identity matrix on  $\mathcal{H}_S$  (infinite temperature state) in a local singlet configuration that maximally entangles every physical site with its auxiliary duplicate, and then applying imaginary time-evolution [13] to obtain the purified state  $|\psi\rangle$  at finite temperature, now living in a total Hilbert space with  $N = N_S + N_A = 2N_S$  sites. This state is then perturbed by a spin flip operator  $Y = X_c$  acting on the central site. For assessing the anticipated computational

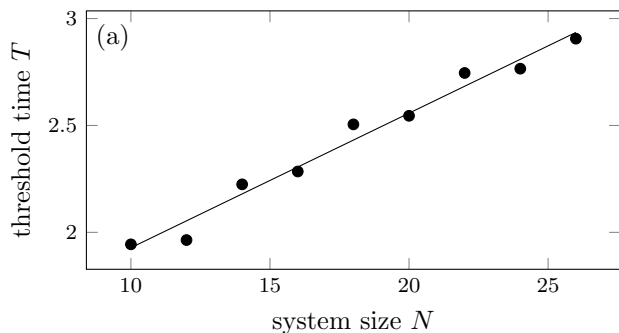


FIG. 3. The threshold passing times  $T$  as a function of system size  $N$  at which  $S_{\text{cb}}$  for plain parallel and Rényi optimization differ by at least  $\epsilon_{\text{thr}} = 0.02$ . The observed linear increase with system size suggests that the deviation between the two approaches is mainly a finite-size effect resulting from excitations that travel from the system center to the open boundaries.

complexity, our quantity of interest is the von Neumann entanglement entropy  $S_i$  across the bond  $i$  connecting the sites  $i$  and  $i + 1$  in a left-right bipartition (see Fig. 1a), defined as  $S_i = -\text{tr}[\rho_i \log \rho_i]$  with  $\rho_i = \text{tr}_{j>i} |\psi\rangle\langle\psi|$  being the reduced density matrix after tracing over sites  $j > i$  on both system and auxiliary. The main focus is then on the half-system bipartition with the central-bond entropy  $S_{\text{cb}}$  as the generic worst case scenario expected to exhibit the largest entanglement entropy, and thus requiring the largest bond dimension  $\chi$  in MPS simulations. We note that there are more detailed representability indicators [44] provided by Rényi entropies across the respective bonds.

In the remainder of this section, we will first present exact numerical data in the framework of ED [45–47] in Section III A to assess at a fully microscopic level the potential of our geometric disentangling approach, independent of any approximations that may be made for practical computational reasons when using TN methods. Afterwards, in Section III B, we generally outline and concretely benchmark for exemplary settings how to harness geometric disentanglers for faster MPS calculations.

### A. Exact Diagonalization Analysis

In order to numerically carry out the parallel transport governed by the auxiliary Hamiltonian  $G$ , we may rewrite Eq. (11) in terms of the initial purification  $w$  as

$$\tilde{G} = -2 \int_0^\infty d\tau e^{-w^\dagger w \tau} w^\dagger H w e^{-w^\dagger w \tau}, \quad (21)$$

so as to avoid the polar decomposition required to compute  $\sqrt{\rho(0)}$ . The explicit evaluation of the integral in Eq. (21) may also be circumvented by obtaining the auxiliary Hamiltonian  $\tilde{G}$  in Eq. (21) directly from the corresponding Lyapunov equation

$$\tilde{A} \tilde{G} + \tilde{G} \tilde{A} + \tilde{Q} = 0, \quad (22)$$

where  $\tilde{A} = -w^\dagger w$ ,  $\tilde{Q} = -2w^\dagger H w$ . Parallel transport is then described by the time-evolution  $t \mapsto w(t) = e^{-iHt} w e^{-i\tilde{G}t}$ , now acting directly on the initial purification  $w$ . The MPS data for the Rényi disentangler [25] to which we compare our geometric approach is obtained with the help of the tensor network package TeNPy (0.10.0) [48]. Convergence of the different results is checked by monitoring the Fröbenius norm difference of the physical density matrices  $\rho(t)$  so as to make sure that only different gauge transformations are compared while maintaining the exact physical time-evolution to high precision in all calculations.

*Finite size effects.* While the Rényi disentangler and parallel transport exhibit very similar entanglement properties regarding  $S_{\text{cb}}$  for large systems (cf. Fig. 1b), in our ED simulations we notice that the two disentanglers start to deviate significantly at finite times that tend to increase with system size. We suspect this to occur at times when the open boundaries of the system become visible to excitations spreading from the center at a certain velocity  $v$ . To verify this intuition, we consider the deviation of plain parallel transport and local Rényi optimization given by the accumulated  $L^2$  norm distance of two paths  $\gamma$  and  $\sigma$  at time  $t$

$$d(\gamma, \sigma, t) = \sqrt{\int_0^t d\tau [S_{\text{cb}}(w_\gamma(\tau)) - S_{\text{cb}}(w_\sigma(\tau))]^2}. \quad (23)$$

By comparing the times  $T$  after which this distance passes a certain threshold, i.e.  $d(\gamma, \sigma, T) \geq \epsilon_{\text{thr}}$ , for  $\gamma$  corresponding to parallel transport and  $\sigma$  to local Rényi optimization, we measure the times up to which the two approaches approximately concur for varying system size. The linear increase of  $T$  with system size indicated by the data shown in Fig. 3 is indeed compatible with the physical picture of a light-cone hitting the open boundaries at  $vT = N_S/2$ . This suggests that the skew corrections in the entanglement landscape described by Eq. (19) may be small at  $\beta = 0.2$  (unless systematically missed also by the Rényi disentangler) on the time-scales relevant for numerical simulations of large systems, i.e. until the open boundaries become visible in the data as a significant finite-size effect.

*Accounting for skew corrections.* Next, in the aforementioned finite size regime where local Rényi optimization can outperform plain parallel transport, we explicitly compute the skew corrections introduced in Eq. (19), thus demonstrating that entanglement can in principle be reduced by geometric means even significantly below the values achieved with Rényi optimization. To this end, we parameterize the vertical tangent space along the fibers (see Fig. 2) using a full basis of Hermitian matrices acting on  $\mathcal{H}_A$  as generators  $g_i$ , and compute the full Hessian in Eq. (19). Solving the linear system using GMRES [49] [50] then allows us to study the effects of the skew correction. Specifically, the numerical data shown in Fig. 4 clearly shows an additional reduction of  $S_{\text{cb}}$  compared to both plain parallel transport and local Rényi optimization.



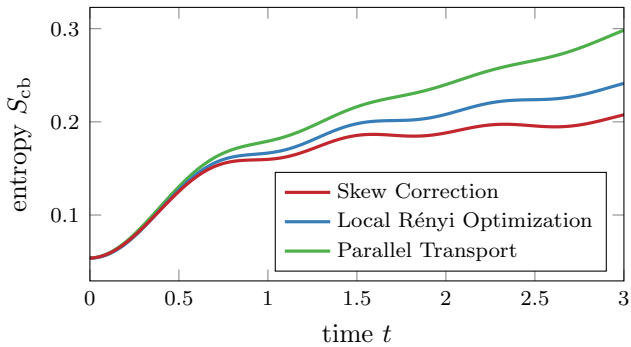


FIG. 4. The entropy  $S_{cb}$  across the central bond of the chain compared for the TFI chain at  $N = 12$  sites for various disentanglers, showing the improvement obtainable by correcting for the skewing of the entanglement landscape. The initial entanglement entropy was optimized using gradient descent for the initial purification to be locally minimal.

However, we note that the exact computation of skew corrections is limited to small systems due to the exponential growth in system size of the number  $\mathcal{N}_g = \dim(\mathcal{H}_A)^2$  of generators  $g_i$  of the unitary group  $U(\dim(\mathcal{H}_A))$  of eligible disentangling transformations. Still, computing skew corrections is much more viable than brute force global optimization of  $U_A(t)$ , which would even scale exponentially in the already exponentially big number  $\mathcal{N}_g$ . In Section IIIB, we will outline how skew corrections may be used at least approximately to go beyond plain parallel transport in MPS simulations.

*Viability regime of the temperature limits.* The two limits to Eq. (11) for zero temperature ( $\beta = \infty$ ) and infinite temperature ( $\beta = 0$ ) are viable at different temperatures regimes as shown in Fig. 5. If the respective regimes are not known, the plain parallel transport is an effective guess, while for both low and high temperature its limits are better suited as mitigating entanglement growth due to their approximate inclusion of skew corrections.

## B. Matrix Product State Benchmark

The variational framework of TN methods in general and MPS as the most widely used TN ansatz designed for one-dimensional systems in particular have advanced to an important part of the computational toolbox in recent years. TN states provide a numerically unbiased method where the main bottleneck lies in the exponential cost with increasing entanglement entropy of the parametrized states. Mitigating the dynamical growth of entanglement in quantum time evolution is thus an important program for extending the range of classical computers regarding the simulation of quantum many-body systems. In the following, we investigate as to what extent our present geometric disentangler approach can practically contribute to this program by performing MPS simulations on the model defined in Eq. (20) and comparing their performance to previous disentangling approaches.

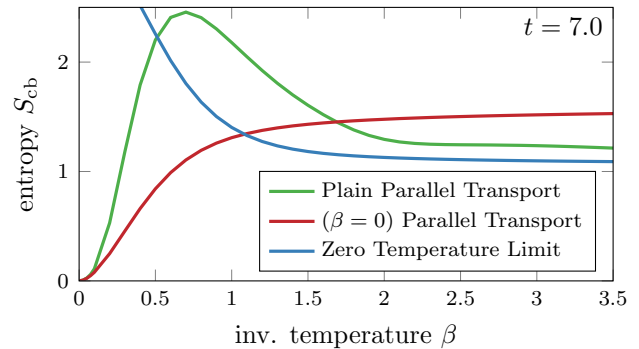


FIG. 5. The central-bond entropy  $S_{cb}$  at  $t = 7.0$  compared for the plain parallel transport compared to its infinite temperature ( $\beta = 0$ ) and zero temperature ( $\beta = \infty$ ) limit, showing the large viability regime of the respective approximations. The data is obtained from ED calculations at  $N = 26$  sites.

A pure (or purified) state  $|\psi\rangle$  on a lattice comprised of  $N$  sites with open boundary conditions and local basis states  $|\sigma_i\rangle$  can be expressed as a MPS [13, 51] by decomposing its wavefunction into tensors  $A_i^{\sigma_i}$  such that

$$|\psi\rangle = \sum_{\{\sigma_i\}} A_1^{\sigma_1} \cdots A_L^{\sigma_L} |\sigma_1 \dots \sigma_L\rangle. \quad (24)$$

For states with sub-extensive entanglement entropy, e.g. for area law entangled states [52], this construction allows to reach values of  $N$  far beyond the scope of ED, because the required matrix size (bond-dimension) of the tensors  $A_i^{\sigma_i}$  grows sub-exponentially with system size. Remarkably, for ground states of one-dimensional systems with an energy gap and thus a finite correlation length, the required bond dimension asymptotically does not grow at all with  $N$  [53], thus allowing to solve arbitrary big systems with MPS methods such as the density matrix renormalization group (DMRG) [17]. Generic operators are included in this framework by decomposing them in a similar manner to obtain a matrix product operator (MPO), e. g. for the Hilbert-Schmidt operator representation  $w$  of the purified state. Importantly, purifications of generic thermal states only contain area law spatial entanglement and can thus be efficiently represented as MPS [54]. This property makes them superior to other approaches such as minimally entangled typical thermal states (METTS) [55] for our present context of computing dynamical finite-temperature correlation functions. The main challenge is then to mitigate by means of the disentangler  $U_A(t)$  (see Fig. 1a) the dynamical growth of entanglement in the time-evolution after the equilibrium state has been perturbed by a local operator inducing the quasi-particle like propagation of entanglement [56].

*Parallel Transport for MPS.* To realize parallel transport in the MPS framework, we notice that the Lyapunov equation, Eq. (12), can be vectorized rather naturally in the MPS framework. Based on this observation, we introduce a Krylov-subspace [57] based approach to Eq. (22),

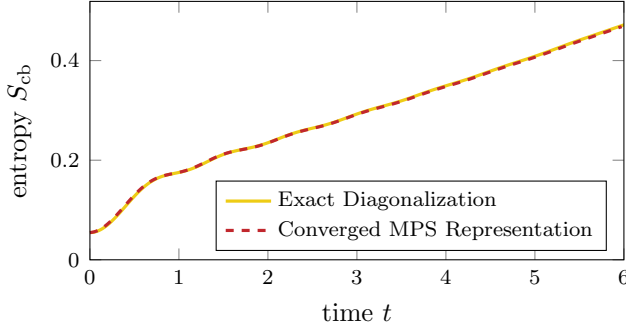


FIG. 6. Comparison between the central bond entropy  $S_{cb}$  with the plain parallel transport disentangler obtained from ED and the iterative GMRES method for MPS (cf. Eq. (25)) at  $N = 26$  sites, showing perfect agreement between the two, obtained already after one sweep in Eq. (25).

by solving the vectorized matrix equation

$$\left( \begin{array}{c} \tilde{A} \otimes \mathbb{I} + \mathbb{I} \otimes \tilde{A} \\ \text{---} \end{array} \right) \text{vec } \tilde{G} = - \text{vec } \tilde{Q} \quad (25)$$

The equation is represented using tensor network diagrams. On the left, a large circle is formed by two smaller circles (representing  $\tilde{A} \otimes \mathbb{I} + \mathbb{I} \otimes \tilde{A}$ ) connected by horizontal lines. This is set equal to the negative of a diagram on the right, which consists of a hexagon and a rectangle connected by lines. The diagram uses circles for MPO tensors ( $\tilde{A}$ ), hexagons for  $\tilde{G}$ , and rectangles for  $\tilde{Q}$ . Solid lines are legs, dotted lines are links, and dashed lines represent the identity.

where the different shapes (circle, hexagon and rectangle) correspond to the tensors of the respective MPO ( $\tilde{A}$ ,  $\tilde{G}$  and  $\tilde{Q}$ ) with solid lines denoting their legs, dotted lines their links and dashed lines being the identity. The equation is solved using the iterative Krylov method GMRES [49] applied to the MPS, which is known in the DMRG context from the correction vector method [58, 59]. Our practical implementation is based on the TN library ITensor [60, 61]. The resulting auxiliary Hamiltonian  $\tilde{G}$  obtained from Eq. (25) reproduces the exact results, as is shown in Fig. 6, thus demonstrating how parallel transport can be implemented efficiently in the MPS framework. The numerical data on a total system size of  $N = 200$  shown in Fig. 1b then exemplifies how parallel transport disentanglers can be harnessed in larger scale MPS simulations. There, the geometric disentangler comes at a similar overhead cost to the simple backward time evolution approach, while at least matching the performance in entanglement mitigation of the inherently much more costly Rényi disentangler. More specifically, the main advantage of the parallel transport approach is that  $\tilde{G}$  may be computed once for a given initial condition and physical Hamiltonian  $H$ , and then be used for various simulations. By contrast, the Rényi disentangler involves solving a non-linear optimization problem at each time-step of every simulation. If this “compute once use many times” character of  $\tilde{G}$  is not applicable in some computational scenario, e.g. for a time-dependent physical Hamiltonian, complementary to our present approach of solving a Lyapunov equation, parallel transport

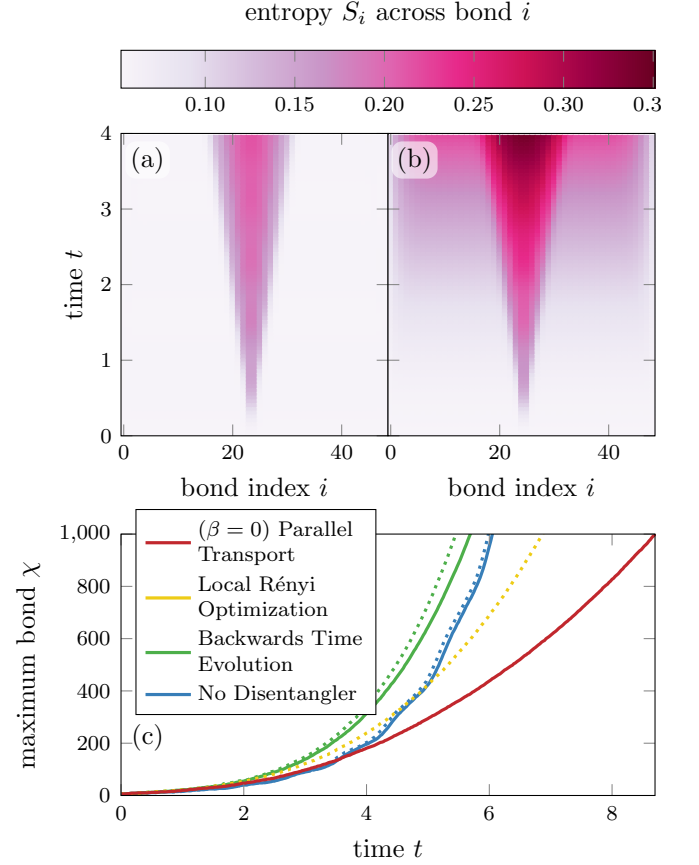


FIG. 7. (a) - (b) Spatio-temporal entanglement landscape of a thermal initial state perturbed by a central spin flip  $X_c$  at  $t = 0$  for the TFI model given in Eq. (20) with a total system size of  $N = 100$  sites, comparing the parallel transport disentangler (a), and the Rényi disentangler (b). In panel (c), the required maximum bond dimension to faithfully represent the purification under time evolution with different disentanglers computed in TeNPy (dotted) and ITensor (solid) is depicted.

may also be implemented on the fly based on singular value decomposition in every time step as outlined in Appendix A.

A complementary approach to computing  $\tilde{G}$  given by direct numerical evaluation of Eq. (11) in the MPS framework is discussed in Appendix B. However, we found the above Krylov-subspace approach to the Lyapunov equation to be drastically superior, since it is both numerically more stable and requires significantly less computational resources due to its fast convergence.

*Infinite temperature approximation.* From Fig. 5, approximating  $\tilde{G}$  by its infinite temperature value (see Eq. (16)) even at finite temperatures may be a promising and straightforward way to utilize parallel transport in existing MPS code. This amounts to applying the conjugate operator  $Y^\dagger$  on the mirrored site in the auxiliary degrees of freedom and evolving the state using the system Hamiltonian. This simple approximation may already lead to a substantial speedup of TN simulations



as is demonstrated in Fig. 7. This is reflected in both the entanglement entropy (cf. Figs. 7a and 7b), showing comparable (lower) entanglement entropy as the local Rényi entropy optimization, and also in a significantly lower required maximum bond dimensions compared to all the previous approaches at the same precision (cf. Fig. 7c).

*Outlook on approximate skew corrections.* In Fig. 4, we have shown that including skew corrections (cf. Eq. (19)) to parallel transport may lead to significant further improvements, at least in a finite size regime. However, exactly including skew corrections in MPS simulations of large systems to us seems computationally unviable. To address this issue, we now outline how skew corrections might be used at an approximate level, the implementation of which is beyond the scope of this work. Inspired by variational cluster approximations (VCA) [62, 63], we propose to solve exactly for skew corrections on small clusters of auxiliary sites (the data in Fig. 4 corresponds to  $N_A = 6$  auxiliary sites) at every time step, and combine the corrections from different time steps to a “brick-wall” of correcting unitaries along the lines of the Rényi disentangler approach [25]. An advantage to VCA methods is that imperfections of this local approximation do not directly lead to incorrect physical results but only limit the performance of the disentangling gauge transformation in mitigating the computational cost from dynamical entanglement growth. This advantage is shared by the local (two-site) approximation of the Rényi disentangler, of course. Yet, while the latter approach solves an optimization problem brute force at every time-step, skew corrections make use of geometric insights that lead to a better scaling with cluster size than a global optimization approach (see discussion in Section III A).

#### IV. CONCLUDING DISCUSSION

We have demonstrated the far reaching potential of geometric disentanglers towards taming the dynamical entanglement growth in purified quantum many-body states. To this end we have first presented a general analysis on the relation between the differential geometry of the Hilbert-Schmidt bundle of purifications and disentangling gauge transformations for extending the scope of classical simulations on the dynamics of mixed quantum states. Based on this theoretical backbone, we have analyzed the practical performance of geometric disentanglers for computing dynamical (real time/frequency) equilibrium response functions of a paradigmatic non-integrable spin chain model with both ED and MPS simulations.

In summary, our geometric approach may be applied at three levels of sophistication. First and most simply, at high temperatures the infinite temperature limit of Uhlmann parallel transport may be used as a disentangler, the generator of which can be expressed exactly without causing computational overhead. Second, for time-independent physical Hamiltonians, at any finite temperature the time-independent generator of Uhlmann

parallel transport can be efficiently computed as an MPO by solving a vectorized Lyapunov equation, and then be used as a geometric disentangler for real-time evolution. Third, at finite temperature, our theoretical analysis indicates that plain parallel transport, while going a long way in mitigating entanglement growth, generically does not provide the optimal disentangler. Instead, higher order skew corrections to parallel transport are shown with ED simulations to significantly reduce entanglement further, at least at times where finite size effects become important. However, these skew corrections in our understanding cannot be efficiently implemented in MPS simulations at a numerically exact level. To address this issue, we have outlined how cluster approximations to skew corrections may allow to tap at least some of their additional potential in future TN algorithms.

To assess the practical added value in the field of computational physics of our general results, we have compared the performance of geometric disentanglers to other well established methods aiming at mitigating entanglement growth in purifications. In all investigated scenarios, our approach is at least competitive with previously proposed disentanglers, and is found to outperform its direct alternatives in a range of settings including the long-time regime at high temperature. The latter regime is of particular importance since disentanglers can make the biggest difference there. This is because a warm to hot physical state is very far from a pure state, for which the gauge-ambiguity of purification and with that the entire disentangling issue perishes. Furthermore, accessing late times represents the fundamental bottle neck since the residual linear entanglement growth, however small its velocity, eventually builds up an exponential wall.

#### ACKNOWLEDGMENTS

We acknowledge discussions with Sebastian Diehl and David Luitz as well as financial support from the German Research Foundation (DFG) through the Collaborative Research Centre SFB 1143 (Project-ID 247310070), the Cluster of Excellence ct.qmat (Project-ID 390858490). Our numerical calculations have been performed at the Center for Information Services and High Performance Computing (ZIH) at TU Dresden.

#### Appendix A: Numerical Time-Stepping Approach to Parallel Transport

A numerical on the fly approach to solving Eq. (8) is obtained along the following lines [31, 64]. Consider the path  $\gamma : t \mapsto w(t)$  at times  $t$  and  $t + \epsilon$  for small  $\epsilon$ . Then Eq. (8) turns into the finite difference equation

$$w^\dagger(t + \epsilon)w(t) - w^\dagger(t)w(t + \epsilon) = 0. \quad (\text{A1})$$

For  $X = w^\dagger(t + \epsilon)w(t) = U^\dagger(t + \epsilon)\sqrt{\rho(t + \epsilon)}\sqrt{\rho(t)}U(t)$ , parallel transport requires  $X = X^\dagger$ . This can be used

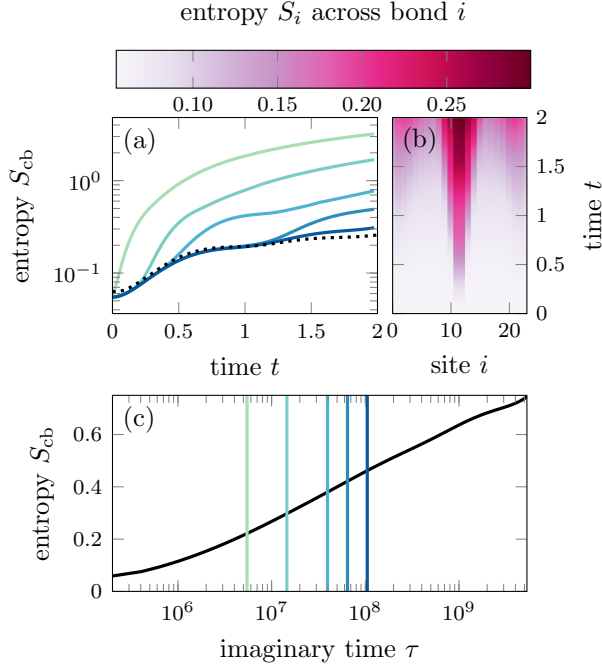


FIG. 8. Slow convergence behavior of the entanglement entropy  $S_{cb}$  under time evolution with the parallel transport Hamiltonian  $\tilde{G}$  obtained from the integral Eq. (B1) at  $N = 50$  sites in the MPS framework. In (a) the bottlenecking entanglement entropy across the center cut is shown to decrease with larger maximum integration time (at times shown as vertical lines in (c)) ultimately leading to the entanglement landscape in (b). The entanglement entropy of the MPS  $T(\tau)$  (cf. Eq. (B2)) is shown in (c).

numerically to construct the unitaries  $U(t + \epsilon)$  satisfying the parallel transport by inserting the singular value decomposition  $\sqrt{\rho(t + \epsilon)}\sqrt{\rho(t)} = L\Sigma R^\dagger$  with  $L, R^\dagger$  unitary and  $\Sigma$  diagonal. This yields

$$X = U^\dagger(t + \epsilon)L\Sigma R^\dagger U(t), \quad (\text{A2})$$

which is Hermitian if  $U^\dagger(t + \epsilon)L = U^\dagger(t)R$ , or alternatively if the accumulated phase  $U(t + \epsilon)$  satisfies

$$U(t + \epsilon) = LR^\dagger U(t). \quad (\text{A3})$$

## Appendix B: The Integral Form of the Disentangling Hamiltonian

A complementary approach to computing the parallel transport generator  $\tilde{G}$  is based on the numerical evaluation of the integral in Eq. (21), which amounts to contracting and integrating the tensor network

$$\tilde{G} = -2 \int_0^\infty d\tau \quad \begin{array}{c} T(\tau) \quad H \quad T(\tau)^\dagger \\ \text{---} \end{array} \quad (\text{B1})$$

with the  $T(\tau)$  tensor

$$T(\tau) \equiv \exp \left( -\tau \begin{array}{c} w \quad w^\dagger \\ \text{---} \end{array} \right) \quad (\text{B2})$$

Computing this tensor network effectively amounts to performing an imaginary time evolution on  $w$  with the pseudo Hamiltonian  $ww^\dagger$ , which can be realized using time-dependent variational principle (TDVP) [19]. The integral in Eq. (B1) can be accomplished numerically by the midpoint rule. While the computation of  $T(\tau)$  involves only an imaginary time-evolution and is in principle efficiently doable [54], the integral converges very slowly due to the flat spectrum of  $ww^\dagger$  as shown in Fig. 8. Yet, Fig. 8 nicely illustrates how the parallel transport disentangler becomes competitive with the Rényi disentangler on better and better convergence, in agreement with Fig. 1b.

[1] C. H. Bennett, D. P. DiVincenzo, J. A. Smolin, and W. K. Wootters, Phys. Rev. A **54**, 3824 (1996).  
[2] M. Horodecki, Quantum Inf. Comput. **1**, 3 (2001).  
[3] M. M. Wilde, *Quantum Information Theory* (Cambridge University Press, 2013).  
[4] J. Preskill, Quantum computing and the entanglement frontier (2012), arXiv:1203.5813 [quant-ph].  
[5] A. Elben, R. Kueng, H.-Y. R. Huang, R. van Bijnen, C. Kokail, M. Dalmonte, P. Calabrese, B. Kraus, J. Preskill, P. Zoller, and B. Vermersch, Phys. Rev. Lett. **125**, 200501 (2020).

[6] Google Quantum AI and Collaborators, Phase transition in random circuit sampling (2023), arXiv:2304.11119 [quant-ph].  
[7] Y. Kim, A. Eddins, S. Anand, K. X. Wei, E. van den Berg, S. Rosenblatt, H. Nayfeh, Y. Wu, M. Zaletel, K. Temme, and A. Kandala, Nature **618**, 500 (2023).  
[8] L. Amico, R. Fazio, A. Osterloh, and V. Vedral, Reviews of modern physics **80**, 517 (2008).  
[9] V. Alba and P. Calabrese, Proceedings of the National Academy of Sciences **114**, 7947 (2017), <https://www.pnas.org/doi/pdf/10.1073/pnas.1703516114>.

- [10] F. Verstraete, J. J. García-Ripoll, and J. I. Cirac, Phys. Rev. Lett. **93**, 207204 (2004).
- [11] M. A. Nielsen and I. L. Chuang, *Quantum Computation and Quantum Information: 10th Anniversary Edition* (Cambridge University Press, 2010).
- [12] B. M. Terhal, M. Horodecki, D. W. Leung, and D. P. DiVincenzo, Journal of Mathematical Physics **43**, 4286 (2002).
- [13] U. Schollwöck, Annals of Physics **326**, 96 (2011).
- [14] With  $D = \dim(\mathcal{H}_A)$ , the gauge group  $U(D)$  has  $D^2$  real parameters, where  $D$  is typically exponentially large in the physical system size. For dynamical problems,  $U_A(t)$  may be seen as a local gauge transformation in time.
- [15] The EOP in Ref. [12] is defined with respect to a minimization of both the  $U_A$  and the extension  $\mathcal{H}_A$  itself, while in our case  $\mathcal{H}_A$  is fixed. This is however only a technicality since an expansion of the auxiliary Hilbert space does not come with increased EOP as long as  $\mathcal{H}_A$  is sufficiently large [30].
- [16] M. B. Hastings, Journal of Statistical Mechanics: Theory and Experiment **2007**, P08024 (2007).
- [17] S. R. White, Phys. Rev. Lett. **69**, 2863 (1992).
- [18] G. Vidal, J. I. Latorre, E. Rico, and A. Kitaev, Phys. Rev. Lett. **90**, 227902 (2003).
- [19] J. Haegeman, J. I. Cirac, T. J. Osborne, I. Pižorn, H. Verschelde, and F. Verstraete, Phys. Rev. Lett. **107**, 070601 (2011).
- [20] S. Paeckel, T. Köhler, A. Swoboda, S. R. Manmana, U. Schollwöck, and C. Hubig, Annals of Physics **411**, 167998 (2019).
- [21] C. Karrasch, J. H. Bardarson, and J. E. Moore, New Journal of Physics **15**, 083031 (2013).
- [22] T. Barthel, New Journal of Physics **15**, 10.1088/1367-2630/15/7/073010 (2013).
- [23] N. Schuch, M. M. Wolf, F. Verstraete, and J. I. Cirac, Physical Review Letters **100**, 10.1103/physrevlett.100.030504 (2008).
- [24] C. Karrasch, J. H. Bardarson, and J. E. Moore, Phys. Rev. Lett. **108**, 227206 (2012).
- [25] J. Hauschild, E. Leviatan, J. H. Bardarson, E. Altman, M. P. Zaletel, and F. Pollmann, Phys. Rev. B **98**, 235163 (2018).
- [26] A. Uhlmann, Reports on Mathematical Physics **24**, 229 (1986).
- [27] A. Uhlmann, Reports on Mathematical Physics **33**, 253 (1993).
- [28] The Schmidt-theorem [30, 65] requires that  $\dim \mathcal{H}_A \geq \dim \mathcal{H}_S$  for an arbitrary state to be representable using a purification. Therefore, a choice with  $\dim \mathcal{H}_A = \dim \mathcal{H}_S$  is sufficient.
- [29] The set  $\{|\phi_i\rangle\}$  refers to a basis of the system Hilbert space  $\mathcal{H}_S$ , while  $\{|\alpha_i\rangle\}$  ( $\{\langle\alpha_i|\}$ ) refers to a basis of the auxiliary Hilbert space  $\mathcal{H}_A = \mathcal{H}_S$  ( $\mathcal{H}_A = \mathcal{H}_S^*$ ).
- [30] I. Bengtsson and K. Życzkowski, *Geometry of Quantum States: An Introduction to Quantum Entanglement* (Cambridge University Press, 2006).
- [31] J. C. Budich and S. Diehl, Physical Review B **91**, 10.1103/physrevb.91.165140 (2015).
- [32] M. V. Berry, Proceedings of the Royal Society of London. A. Mathematical and Physical Sciences **392**, 45 (1984).
- [33] J. Dittmann and G. Rudolph, Journal of Geometry and Physics **10**, 93 (1992).
- [34] O. Viyuela, A. Rivas, and M. A. Martin-Delgado, 2D Materials **2**, 034006 (2015).
- [35] M. Fannes, Communications in Mathematical Physics **31**, 291 (1973).
- [36] M. A. Nielsen, Physical Review A **61**, 10.1103/physreva.61.064301 (2000).
- [37] K. M. R. Audenaert, Journal of Physics A: Mathematical and Theoretical **40**, 8127 (2007).
- [38] D. Bures, Transactions of the American Mathematical Society **135**, 199 (1969).
- [39] A. Uhlmann, The metric of bures and the geometric phase, in *Groups and Related Topics: Proceedings of the First Max Born Symposium*, edited by R. Gielera, J. Lukierski, and Z. Popowicz (Springer Netherlands, Dordrecht, 1992) pp. 267–274.
- [40] D. Kennes and C. Karrasch, Computer Physics Communications **200**, 37 (2016).
- [41] S. Paeckel, T. Köhler, A. Swoboda, S. R. Manmana, U. Schollwöck, and C. Hubig, Annals of Physics **411**, 167998 (2019).
- [42] R. Rausch, R. Peters, and T. Yoshida, New Journal of Physics **23**, 10.1088/1367-2630/abd35e (2020).
- [43] R. Peters and R. Rausch, SciPost Physics **14**, 10.21468/SCIPOSTPHYS.14.6.166 (2023).
- [44] F. Verstraete and J. I. Cirac, Physical Review B **73**, 10.1103/physrevb.73.094423 (2006).
- [45] J. Bezanson, A. Edelman, S. Karpinski, and V. B. Shah, SIAM Review **59**, 65 (2017).
- [46] P. K. Mogensen and A. N. Riseth, Journal of Open Source Software **3**, 615 (2018).
- [47] P. Virtanen, R. Gommers, T. E. Oliphant, M. Haberland, T. Reddy, D. Cournapeau, E. Burovski, P. Peterson, W. Weckesser, J. Bright, S. J. van der Walt, M. Brett, J. Wilson, K. J. Millman, N. Mayorov, A. R. J. Nelson, E. Jones, R. Kern, E. Larson, C. J. Carey, Í. Polat, Y. Feng, E. W. Moore, J. VanderPlas, D. Laxalde, J. Perktold, R. Cimrman, I. Henriksen, E. A. Quintero, C. R. Harris, A. M. Archibald, A. H. Ribeiro, F. Pedregosa, P. van Mulbregt, and SciPy 1.0 Contributors, Nature Methods **17**, 261 (2020).
- [48] J. Hauschild and F. Pollmann, SciPost Phys. Lect. Notes **5** (2018), code available from <https://github.com/tenpy/tenpy>, arXiv:1805.00055.
- [49] Y. Saad and M. H. Schultz, SIAM Journal on Scientific and Statistical Computing **7**, 856 (1986), <https://doi.org/10.1137/0907058>.
- [50] Using an MINRES algorithm in this case is a necessary, since the solution to Eq. (19) is not unique. This is due to the fact, that junctions in the entanglement landscape can occur.
- [51] D. Perez-Garcia, F. Verstraete, M. M. Wolf, and J. I. Cirac, Matrix product state representations (2007), arXiv:quant-ph/0608197 [quant-ph].
- [52] J. Eisert, M. Cramer, and M. B. Plenio, Rev. Mod. Phys. **82**, 277 (2010).
- [53] U. Schollwöck, Reviews of Modern Physics **77**, 259 (2005).
- [54] T. Barthel, One-dimensional quantum systems at finite temperatures can be simulated efficiently on classical computers (2017), arXiv:1708.09349 [quant-ph].
- [55] M. Binder and T. Barthel, Physical Review B **92**, 125119 (2015).
- [56] P. Calabrese and J. Cardy, Journal of Physics A: Mathematical and Theoretical **42**, 504005 (2009).
- [57] A. Krylov, Izv. Akad. Nauk. SSSR Otd Mat. Estest **1**, 491 (1931).

- [58] T. D. Kühner and S. R. White, Phys. Rev. B **60**, 335 (1999).
- [59] A. Nocera and G. Alvarez, Physical Review E **94**, 10.1103/physreve.94.053308 (2016).
- [60] M. Fishman, S. White, and E. Stoudenmire, SciPost Physics Codebases 10.21468/scipostphyscodeb.4 (2022).
- [61] M. Fishman, S. R. White, and E. M. Stoudenmire, SciPost Phys. Codebases , 4 (2022).
- [62] A. Georges, G. Kotliar, W. Krauth, and M. J. Rozenberg, Rev. Mod. Phys. **68**, 13 (1996).
- [63] M. Potthoff, M. Aichhorn, and C. Dahnken, Physical review letters **91**, 206402 (2003).
- [64] Z. Huang and D. P. Arovas, Physical Review Letters **113**, 10.1103/physrevlett.113.076407 (2014).
- [65] D. Viennot, Purification of lindblad dynamics, geometry of mixed states and geometric phases (2018), arXiv:1508.02279 [math-ph].